Effects of asymmetric galactic bars on radial velocity maps

Author: Toni Soler Terricabras
Facultat de Física, Universitat de Barcelona, Diagonal 645, 08028 Barcelona, Spain.

Advisor: Mercè Romero-Gómez

Abstract: This study aimed to determine the effects of asymmetric bars on the kinematic behaviour of the inner regions of barred galaxies using test particle simulations. The results of the work suggest that a galactic bar with a deviation of the centre of mass produces asymmetries in the quadrupole signature of radial velocity maps, with the modulus of v_r being larger in the direction of larger mass. It has been further confirmed that the larger the displacement of the centre of mass, the more significant the asymmetries in the radial velocity there are. As an application, this study confirms that the LMC has an asymmetric galactic bar and, for the first time, links this asymmetry in density with the asymmetry found in the galactic maps, as previously suggested by observations from the *Gaia* mission (ESA).

I. INTRODUCTION

Apart from being one of the closest galaxies to the Milky Way, the Large Magellanic Cloud (LMC) is also known for the plethora of peculiar properties it displays. These unusual features encompass morphological anomalies of its galactic bar. As an example, prior studies have noted the off-centre position of this stellar bar [1] and its uneven mass distribution [2] [3].

The cutting-edge data provided by the *Gaia* mission (ESA) have revealed strong asymmetries in the internal kinematics of the LMC [3]. Figure 1 presents a radial velocity map of the LMC resulting from *Gaia* data that clearly shows an asymmetric quadrupole. In reviewing the literature, though, no correlation has been found between irregular bars and asymmetric kinematic maps. This is mainly because the LMC is the first galaxy for which 3D kinematic maps are available, thanks to *Gaia*.

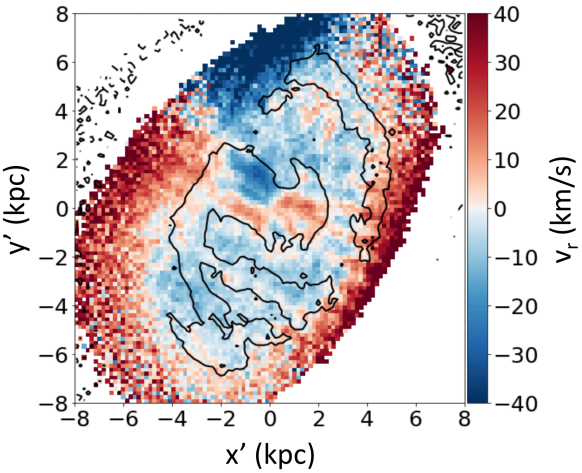

FIG. 1: Median radial velocity map in the LMC coordinate system using the NN Optimal sample without line-of-sight velocity from [3]. Black contours delineate overdensities.

Thus, the main goal of the present study is to determine the effect of asymmetric bars on the kinematic behaviour of the inner regions of barred galaxies by means of test particle simulations. Test particle simulations basically consist on integrating a set of initial conditions under a known galactic potential. They are used to test how a certain property changes when one of the free parameters of the galactic potential is varied. For the sake of our kinematic interest, the property that is examined in our simulations is velocity.

This work is organised as follows. Section II introduces the theoretical models from which our simulations have been devised. It enters into detailed explanation of the different explored strategies to fully analyse this issue. In Section III we present the kinematic analysis of the results from our simulations, showing distinctive orbits and realistic particle distributions. Finally, Section IV summarises the main conclusions of this work.

II. GALACTIC MODELS AND SIMULATIONS

A. Galactic models

Our simulations aim to represent the three-dimensional spatial and kinematic distribution of a realistic generic barred galaxy. Our theoretical model is based on previous papers such as Romero-Gómez et al. (2015) [4]. Essentially, it consists of an Allen & Santillán potential that comprises the axisymmetric component [5] and an added bar-like potential. On the one hand, the axisymmetric potential is defined by a Miyamoto-Nagai disc, a spherical bulge (which we will call *AS-bulge*) and a spherical dark matter halo. Apart from providing a realistic representation of a rotation curve of a disc galaxy, this axisymmetric potential presents the advantage of being completely analytical. On the other hand, the galactic bar has been modelled after a superposition of two Ferrers ellipsoids [6] with non-homogeneity index

of $n = 1$, which we will call *boxy-bulge bar* and *long bar* respectively. Originally, this model was created according to the Milky Way, hence several modifications have been applied –subsection II.B goes into more detail on some of these variations.

The novelty of this work arises from running test particle simulations of galaxies whose bars present an asymmetric density distribution. To do so, we locate a spherical bulge in different displacements. Such scenarios have been considered to represent possible asymmetries that might stem from discrepancies between the bar's geometric centre and its mass centre [7]. Table I compiles the parameters entered for the free values of the potential.

	a (kpc)	b/a	c/a	M $(M_\odot)$
Disc	–	–	–	$8.561 \cdot 10^{10}$
DM halo	–	–	–	$1.071 \cdot 10^{11}$
AS-bulge	–	–	–	$1.406 \cdot 10^{10}$
Boxy-bulge bar	3.13	0.40	0.026	$9.814 \cdot 10^{9}$
Long bar	4.50	0.15	0.026	$4.246 \cdot 10^{9}$
Spherical bulge	–	–	–	$1.406 \cdot 10^{9}$

TABLE I: Semimajor axis, axes ratios and mass of the galactic components.

As a result, the bar mass is $M_B = 1.406 \cdot 10^{10} M_\odot$ [8], the spherical bulge mass is 10% of the AS-bulge mass and the total mass results to be $M_T = 2.082 \cdot 10^{11} M_\odot$ –without the AS-bulge (see subsection II.B). Additionally, the bar is assumed to rotate around the z-axis with a constant pattern speed of $\Omega = 40\, km\, s^{-1}\, kpc^{-1}$[9].

In order to explore this situation, we have run different models in which we changed the geometrical position of the centre of mass of the bar along its semimajor and semiminor axis. Table II summarises the values of the parameters that characterise the five most interesting models that will be presented in this work.

	1	2	3	4	5
Δx (kpc)	0.0	0.2	2.0	0.00	0.0
Δy (kpc)	0.0	0.0	0.0	0.08	0.8

TABLE II: Centre of mass displacement along the x-axis and y-axis respectively in the five models.

Whereas model 1 represents the symmetrical case, models 2-3 and 4-5 have been executed to understand properly the dependencies on displacing the bulge along the semimajor axis and semiminor axis, respectively. For each direction, the bulge has been located around the middle and near the edges of the semiaxes of the boxy-bulge bar, thus creating smaller and larger centre of mass deviations.

B. Integration process

We plan to examine the radial velocity field of each of the models from two viewpoints. Firstly, we want to analyse some periodic orbits, given that they constitute the backbone of galactic bars. For this analysis, initial conditions are integrated in a final time-independent potential. The two main differences between this potential and the Allen & Santillán potential are that the AS-bulge is replaced by a bar with a same mass and that there is an added a spherical bulge –which will create asymmetry.

Secondly, we analyse the radial velocity distribution from a realistic test particle simulation. For the analysis of these kinematic maps, test particles are integrated in a time-dependent potential in order to achieve a relaxed and more realistic situation. At time $t = 0$, the potential exactly corresponds to an Allen & Santillán potential. Thenceforth, this potential is smoothly converted into the aforementioned final potential. As a consequence, for $0 < t < t_{grow}$, the AS-bulge is slowly replaced by a same mass bar while a 10% mass bulge is gradually introduced –meanwhile, both the disc and halo remain static. In particular, this non-axisymmetric component is adiabatically introduced in four bar rotations, i.e. $t_{grow} \approx 0.5 Gyr$. In order to ensure a smooth transition from the non-barred to the barred state, the changeover has been adjusted to the Dehnen [11] fifth degree polynomial $f(\xi) = 6\xi^5 - 15\xi^4 + 10\xi^3$, for $0 < \xi = \frac{t}{t_{grow}} < 1$. Consequently, the centre of mass is gradually changing throughout the potential transition. Finally, once reached the final time-independent potential, we have integrated the conditions for eight more bar rotations to obtain a distribution in statistical equilibrium.

It is worth noting that the data resulting from the simulations are in the Cartesian coordinate system. Therefore, polar velocities can be worked out by applying the following rotation:

$$\begin{pmatrix} v_r \\ v_\phi \end{pmatrix} = \begin{pmatrix} cos\theta & -sin\theta \\ sin\theta & cos\theta \end{pmatrix} \begin{pmatrix} v_x \\ v_y \end{pmatrix} \tag{1}$$

where $\theta = arctan\left(\frac{y}{x}\right)$.

III. RESULTS AND DISCUSSION

A. Kinematics of periodic orbits

We have computed some periodic orbit families in the $x - y$ plane in the aforementioned models since these constitute the backbone of the galactic bar. There are two basic orbital families that are relevant to our case of study, which are x_1 and x_2 orbital families. Both types of orbits are closed and periodic. x_1 orbits are elongated along the major axis of the bar, within corotation, whilst x_2 are perpendicular to the semimajor axis of the bar.

It is known that the bar structure is supported by quasi-periodic orbits trapped around these families [10]. Therefore, we have displayed some of these orbital families in the non-inertial reference frame in the symmetric and asymmetric cases. All the models were integrated for an equal set time of $T = 0.05\,Myr$.

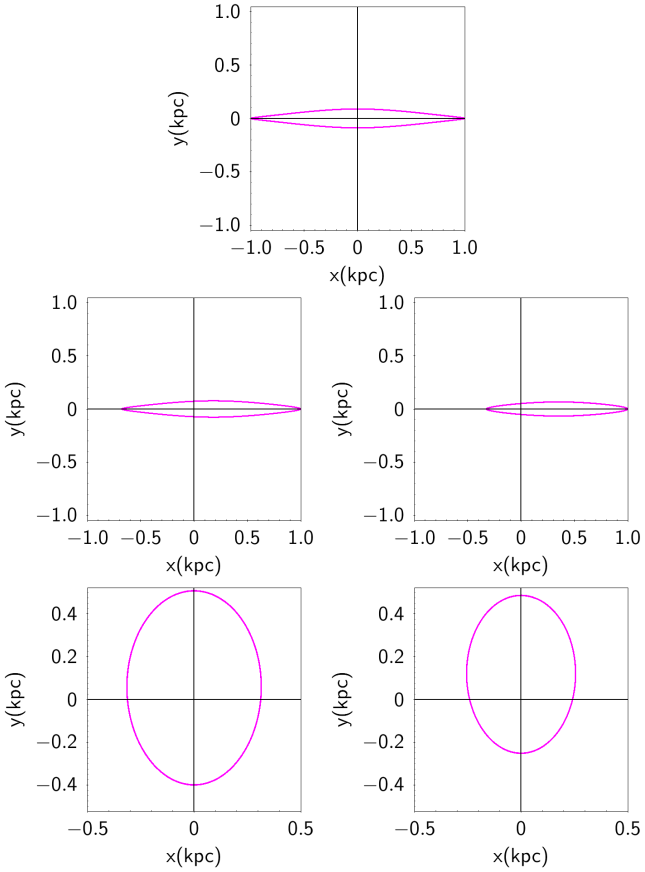

FIG. 2: Selection of periodic orbits. Top: x_1 orbit from model 1. Middle: x_1 orbits from model 2 (left) and model 3 (right). Bottom: x_2 orbits from model 4 (left) and model 5 (right).

Figure 2 shows examples of x_1 and x_2 orbits in the different models. In model 1 (top panel), the orbit is totally symmetrical about both axes. On the contrary, x_1 orbits from models 2 and 3 (middle panels) are shifted along the semimajor axis of the bar. Similarly, models 4 and 5 (bottom panels) display x_2 orbits moved along the semiminor axis. It is immediately noticeable that, the larger the displacement of the bulge, the more off-centre these periodic orbits are.

Given the importance of these types of orbits, we can gain more insight into the dynamics of these systems by analysing their kinematic behaviour. Figure 3 presents the plot of v_x and v_y velocities for the above-mentioned orbits of models 1, 2 and 4. Each plot includes either in red or in blue the radial component of one (arbitrarily chosen) Cartesian velocity vector per quadrant (highlighted in black). Red vectors correspond to positive v_r and blue vectors to negative v_r.

It is clearly perceptible from Figure 3 that model 1 (left pannel) brings about quadrupolar symmetry, in view of the fact that v_r modulus is preserved at a given radius. Red and blue vectors (radial velocity components) appear to have similar moduli. Notwithstanding, in the cases where bulge displacement is applied, this symmetry is not retained. Specifically, we observe that v_r modulus is larger on the quadrants towards which the bulge is moved. In the middle pannel of Figure 3, radial components are more pronounced in quadrants I and IV. In a similar way, in model 4 (right pannel), v_r moduli in quadrants I and II are significantly larger than in quadrants III and IV.

Having seen this behaviour for the main periodic families, we wonder if a similar asymmetry is reproduced when running the simulations with an entire particle distribution. Thus, the driving force behind displaying kinematic maps is to find an asymmetry in radial velocity moduli similar to the observed in these orbits.

B. Analysis of kinematic maps

The kinematic maps presented in this work have been calculated from the test particle simulations described in Section II. We integrate the orbits of a set of $2.4 \cdot 10^6$ initial conditions (x, y, z, v_x, v_y, v_z) generated according to the Appendix A from [4] in both the inertial and non-inertial reference frame for each model. The simulations were run in a desktop computer with six CPUs and the execution time was about twenty-four hours each. The final 6D information (Cartesian positions and velocities) of each particle was stored. Using these ending data, we have created kinematic maps plotting the median v_r in the inertial frame with the TOPCAT [12] plane plot facility in the weighted mode of mark form.

Figures 4 and 5 present the results of running the simulations with the entire set of initial conditions in the time-dependent potential (see Subsection II.B). For the sake of brevity, in this work we only present the kinematic maps of models 1, 3 and 5 given that they present clearer differences in quadrupole signatures. Model 1 (Figure 4) gives rise to a symmetrical quadrupole, as expected. v_r modulus is preserved and keeps similar values in quadrants I-III and II-IV respectively.

Conversely, in the asymmetric cases (Figure 5), v_r is not symmetrical. Model 3 (upper pannel) reveals a strong asymmetry in v_r along the semimajor axis of the bar. There is a weakening of v_r modulus in the quadrupolar components on quadrants II-III. The colours of the outermost parts of the quadrupoles of the aforesaid quadrants appear slightly faded compared

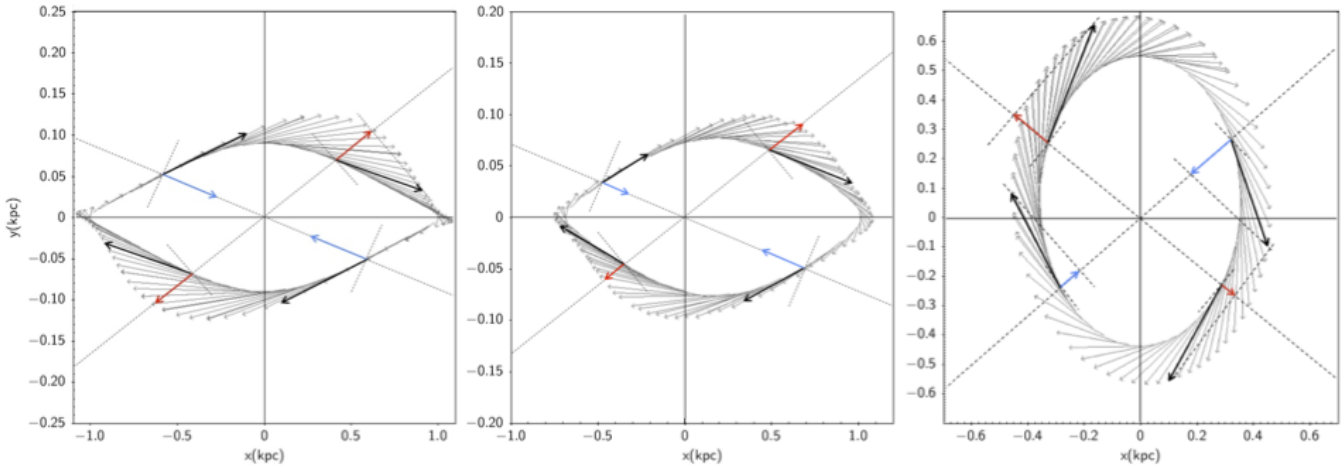

FIG. 3: Planar velocity plot of the periodic orbits for models 1 (left), 2 (middle) and 4 (right). Grey vectors indicate Cartesian velocities whereas coloured (red: positive; blue negative) vectors represent the polar radial component of arbitrarily chosen velocity vectors (black). Axes ratios have been resized for illustrative purposes.

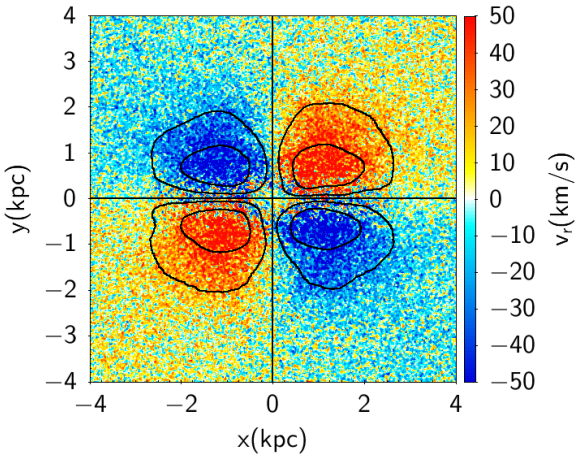

FIG. 4: Median radial velocity map of the N-body simulation from model 1. This map is shown in Cartesian coordinates in the inertial reference frame. It includes isolines of radial velocity that delineate the quadrupole at (-143.2, -51.5, 40.3, 132.0) $km\,s^{-1}$.

with the totally symmetric quadrupole from model 1 (Figure 4). Besides, the isolines tend to shrink inwards in the stated quadrants and slightly expand on the contrary quadrants.

Likewise, the kinematic map resulting from model 5 (lower pannel in Figure 5) presents weaker colours at the lower part of the quadrupole (quadrants III and IV) and its isolines at these regions are compressed towards the y-axis. Moreover, isolines appear more elongated, especially the inner ones. This asymmetry is reasonable given that, in this model, the bulge is displaced along the semiminor axis of the bar.

These findings are consistent with the predictions foretold from the analysis of the kinematics of periodic orbits in Subsection III.A.

We could further argue that the asymmetric kinematic maps obtained from this work are qualitatively comparable to those found by *Gaia* (see Figure 1). To be precise, given that we assume the LMC's galactic bar to have a density peak at one end of the semimajor axis of the bar [3], we would have expected to find a similar quadrupole deformation in model 3 (Figure 5, upper pannel) as in Figure 1. Nevertheless, it is not the case. Note that in Figure 1, the quadrupole is asymmetric along the semiminor axis of the bar, whereas in model 3 (Figure 5, upper pannel), the quadrupole is asymmetric about the semimajor axis of the bar. This rather contradictory result may be due to more complex issues affecting the dynamical behaviour of the galactic bar, for instance, interactions of the LMC with the Small Magellanic Cloud (SMC) and the Milky Way.

IV. CONCLUSIONS

In this work we have studied the kinematic consequences of non-symmetrical bar mass distributions on geometrically centred galactic bars. To do so, we placed a bulge with a 10% mass of the bar in different positions in order to create a deviation of the centre of mass from the geometrical centre of the bar –and, therefore, of the entire galaxy. The results presented in this study are significant in at least two major respects:

- Clearly, a galactic bar with a deviation of the centre of mass provides asymmetric v_r maps. The modulus of radial velocity tends to be larger towards the direction along which the mass is greater.

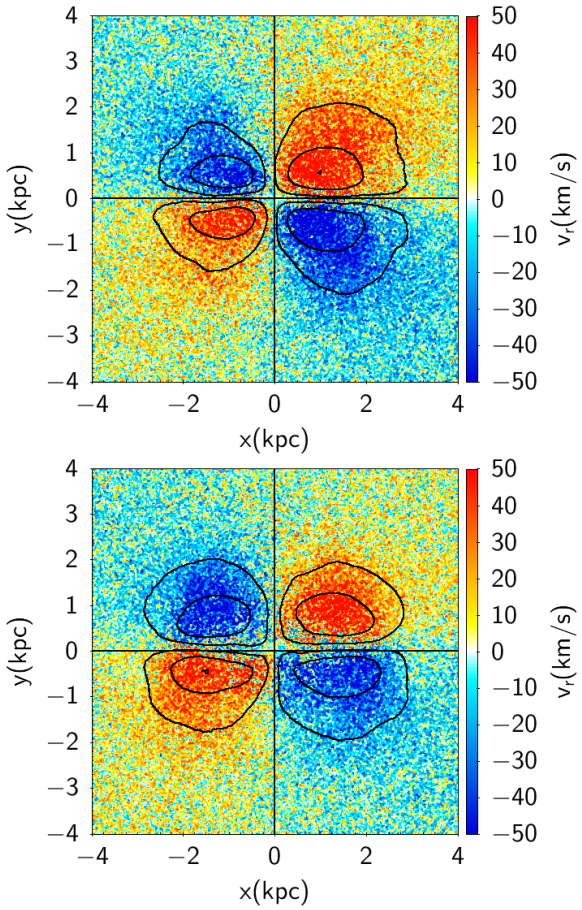

FIG. 5: Median radial velocity maps of N-body simulations from models 3 (top) and 5 (bottom). Both maps are shown in Cartesian coordinates in the inertial reference frame. These maps include isolines of radial velocity (model 3: (-265.9, -92.2, 81.6, 255.4, 429.2) $km\,s^{-1}$; model 5: (-208.3, -66.3, 75.7, 217.7, 359.7) $km\,s^{-1}$) that delineate the quadrupoles.

- The larger the displacement of the centre of mass, the more significant the asymmetries in radial velocity modulus are.

The present study raises the possibility that quadrupolar asymmetries in radial velocity maps of barred galaxies may (at least) stem from displacements of the centre of mass of the galactic bar. In addition, the findings of this work provide solid confirmation for the assumption of the LMC to possess an asymmetric galactic bar, as observed by *Gaia*. On the whole, this study is innovative because it relates asymmetries in kinematic maps to asymmetric galactic bars for the first time.

To develop a more accurate picture of the correlation established in this work, we must include in the analysis the residual tangential velocity component (after subtracting the rotation curve), where we expect analogous results. In future investigations, it might also be possible to use a different approach in which the asymmetry is not generated by an added bulge, but from a geometric displacement of the bar itself. It will doubtlessly add major difficulties in coordinate transformations from inertial to rotational reference frames, yet it may also prove to have satisfactory results.

Acknowledgments

I would like to express my wholehearted gratitude to my advisor Mercè Romero-Gómez for her unwavering support and valuable guidance. Her instructions and assistance have been fundamental to the successful completion of this project. I feel deeply grateful to her for having brought me closer to astronomical research.

[1] De Vaucouleurs, G., et al. "Structure and dynamics of barred spiral galaxies, in particular of the Magellanic type." *Vistas in Astronomy* 14 (1972): 163-294.
[2] Gaia Collaboration: Luri, X., et al. "Gaia Early Data Release 3-Structure and properties of the Magellanic Clouds." Astronomy & Astrophysics 649 (2021): A7.
[3] Jiménez-Arranz, Ó., et al. "Kinematic analysis of the Large Magellanic Cloud using Gaia DR3" arXiv: 2210.01728 (2022).
[4] M. Romero-Gómez, et al., "The analysis of realistic stellar Gaia mock catalogues – I. Red clump stars as tracers of the central bar", *Monthly Notices of the Royal Astronomical Society*, 447, 1 (2015): 218–233.
[5] Allen, C., et al. "An improved model of the galactic mass distribution for orbit computations." *Revista Mexicana de Astronomia y Astrofisica* 22 (1991): 255-263.
[6] Ferrers, N.M. "On the potential of ellipsoids, ellipsoidal shells, elliptc laminae and elliptic rings, of variable densities". Q. J. Pure Appl. Math. (1877): 14, 1–22
[7] Sánchez-Martín, et al. "Formation of asymmetric arms in barred galaxies", in prep. (2023)
[8] Sormani, MC., et al. "The stellar mass distribution of the Milky Way's bar: an analytical model." *Monthly Notices of the Royal Astronomical Society*, 514.1 (2022): 1-5.
[9] Bovy, J., et al. "Life in the fast lane: a direct view of the dynamics, formation, and evolution of the Milky Way's bar." Monthly Notices of the Royal Astronomical Society 490.4 (2019): 4740-4747.
[10] Contopoulos, G., "Order and Chaos in Dynamical Astronomy", *Berlin: Springer (Astronomy and Astrophysics Library)* QB 351.K58 (2002).
[11] Dehnen, W. "The effect of the outer Lindblad resonance of the galactic bar on the local stellar velocity distribution." *The Astronomical Journal* 119.2 (2000): 800.
[12] Taylor, M.B. *TOPCAT: Astronomical Data Analysis Software and Systems XIV* (2005): 347, 29.